Acta Crystallographica Section B
**Structural Science**
ISSN 0108-7681

# Synchrotron X-ray analysis of $RbTiOAsO_4$

**Victor A. Streltsov,[a]* Jenni Nordborg née Almgren[b] and Jörgen Albertsson[b]**

[a]Crystallography Centre, University of Western Australia, Nedlands 6907, Australia, and [b]Inorganic Chemistry, Chalmers University of Technology, SE-412 96 Göteborg, Sweden

Correspondence e-mail: strel@crystal.uwa.edu.au

Received 29 December 1999
Accepted 25 April 2000

Structure factors for rubidium oxotitanium arsenate, $RbTiOAsO_4$, were measured at 293 K with focused synchrotron X-radiation [$\lambda$ = 0.7500 (9) Å] using a fast avalanche photodiode counter. The accurate synchrotron single-crystal data are of sufficient quality and resolution to detect the splitting positions of the Rb cations at room temperature. Strong accumulation of the $\Delta\rho$ difference charge density near the Rb atoms at a distance of ~0.5 Å in the $-c$ direction can be attributed to the partial occupancy of additional sites related by pseudosymmetry. This type of static and/or dynamic disorder is temperature-dependent and seems to be universal for the $KTiOPO_4$ family of compounds. The best modelling of the experimental data was obtained with the Rb atom in split positions described within the harmonic approximation and the multipole functions for the other atoms. The $\Delta\rho$ density features in the Ti—O and As—O covalent bonds can be related to the linear and non-linear susceptibility using bond-polarization theory. The charge-density maps reflect the anisotropy of non-linear susceptibility, which is larger for directions where locally antisymmetric components of $\Delta\rho$ are strong.

## 1. Introduction

Numerous studies of the potassium titanyl phosphate (KTP) family of compounds reflect the high interest in the ferroelectricity and non-linear optical properties of these materials, but the full understanding is not yet complete. Rubidium titanyl arsenate (RTA) is a member of the KTP family. RTA shows much lower ionic conductivity compared with KTP, enabling the periodic poling of flux-grown RTA crystals (Karlsson *et al.*, 1996; Hu *et al.*, 1996; Risk & Loiacono, 1996) which is very important for quasi-phase-matching of non-linear interactions. In addition, RTA has higher transmission in the IR region, which can significantly extend the optical range of lasers (Mangin *et al.*, 1989).

The ferroelectric phase transition in KTP isomorphs is recognized as a continuous second order of both displacive and order–disorder type (*e.g.* Belokoneva *et al.*, 1997). The $T_c$ phase-transition temperature of 1067 K for RTA (Marnier *et al.*, 1989) is lower than that of 1207 K for KTP (Stefanovich *et al.*, 1996). During the transformation from the paraelectric *Pnan* phase to the ferroelectric $Pna2_1$ phase the alkali metal ions are significantly displaced along the polarization vector falling into two independent sites. This suppresses the *Pnan* symmetry and creates polarity along the $2_1$ axis parallel to **c** (Belokoneva *et al.*, 1997). Still, elements of the high-temperature structure are retained at room temperature in KTP and its isomorphs (Thomas *et al.*, 1990; Thomas & Womersley, 1998). When the temperature decreases below

**Table 1**
Experimental details.

| | |
|---|---|
| Crystal data | |
| Chemical formula | $RbTiOAsO_4$ |
| Chemical formula weight | 288.27 |
| Cell setting | Orthorhombic |
| Space group | $Pna2_1$ |
| $a$ (Å) | 13.2352 (11) |
| $b$ (Å) | 6.6666 (7) |
| $c$ (Å) | 10.7483 (9) |
| $V$ (Å$^3$) | 948.36 (15) |
| $Z$ | 8 |
| $D_x$ (Mg m$^{-3}$) | 4.038 |
| Radiation type | Synchrotron X-ray vertical wiggler |
| Wavelength (Å) | 0.75 |
| No. of reflections for cell parameters | 12 |
| $\theta$ range (°) | 42.458–50.782 |
| $\mu$ (mm$^{-1}$) | 21.09 |
| Temperature (K) | 293 |
| Crystal form | Rectangular |
| Crystal size (mm) | 0.064 × 0.058 × 0.040 |
| Crystal colour | Colourless |
| | |
| Data collection | |
| Diffractometer | BL14A four-circle† |
| Data collection method | $\omega$–$2\theta$ scans |
| Absorption correction | Analytical |
| $T_{min}$ | 0.344 |
| $T_{max}$ | 0.494 |
| No. of measured reflections | 46 432 |
| No. of independent reflections | 6310 |
| No. of observed reflections | 5982 |
| Criterion for observed reflections | $F^2 > 0$ |
| $R_{int}$ | 0.0541 |
| $\theta_{max}$ (°) | 60 |
| Range of $h$, $k$, $l$ | $-30 \rightarrow h \rightarrow 30$<br>$-15 \rightarrow k \rightarrow 15$<br>$-24 \rightarrow l \rightarrow 24$ |
| No. of standard reflections | 6 |
| Frequency of standard reflections | Every 94 reflections |
| Intensity decay (%) | 8.8 |
| | |
| Computer programs | |
| Data collection | BL14A software |
| Cell refinement | BL14A software |
| Data reduction | *Xtal DIFDAT ADDREF SORTRF ABSORB* |
| Structure solution | *Xtal* |
| Structure refinement | *Xtal CRYLSQ XD* |
| Preparation of material for publication | *Xtal BONDLA CIFIO XD* |

† The BL14A four-circle diffractometer (Satow & Iitaka, 1989) at the Tsukuba Photon Factory, Japan.

room temperature the alkaline cations move further away from the pseudosymmetric positions (*e.g.* Dahaoui *et al.*, 1999; Almgren *et al.*, 1999). Moreover, Thomas & Womersley (1998) and Womersley *et al.* (1998) reported some evidence of disorder of alkali cations over additional sites along the $c$ direction, particularly for the Cs-rich end of $Cs_xRb_{1-x}TiOAsO_4$ mixed compounds at room temperature. The residual charge-density peaks were observed at the additional sites related by a pseudo-inversion centre to the main sites. The question was posed whether this "'hosting' phenomenon is universal in polar crystals, in general, or even in crystals of the KTP-type structure with different substituent elements". It was concluded that the disordered model is the correct one for mixed crystals, especially with a high content of heavy cations such as Cs. The occupancies of disordered positions for alkali cations were also refined in mixed germanate analogues of KTP measured by high-resolution neutron powder diffraction at different $T > T_{room}$ (Belokoneva *et al.*, 1997).

The crystal model with split K positions has been refined for pure $KFeFPO_4$ and KTP itself from X-ray diffraction experiments at room temperature (Belokoneva *et al.*, 1990). For KTP at room temperature as studied by Hansen *et al.* (1991), the residual charge density around the K atoms after conventional independent atom model (IAM) refinement also showed a pronounced non-spherical surrounding ('ghost' peaks). However, including non-spherical multipole functions at the K sites greatly reduced these features and did so more efficiently than the introduction of an anharmonic Gram–Charlier expansion of the temperature function. In addition, the modelling of the density at the K sites significantly influenced the density near the Ti atoms. Further studies of KTP at 9 K by Larsen (1995) showed that the features near the K atoms became progressively smaller. In fact, the 9 K maps were very close to the room-temperature maps corresponding to a refinement using non-spherical symmetric density functions for K.

Recent detailed X-ray diffraction studies by the authors (Almgren *et al.*, 1999) of a good quality colourless RTA sample at 9 K showed some residual (dipole-like) density near Rb atoms which was very similar to that in KTP at 9 K. Atomic displacements were very small at 9 K and could be described well in the harmonic approximation. Refinement of the structural model with disordered Rb positions was ineffective for the 9 K data.

The evolution to centrosymmetry of the KTP and $RbTiOPO_4$ (RTP) structures was studied by Delarue *et al.* (1998, 1999) using X-ray diffraction data in the temperature range 293–973 K. Best fits were obtained using two refinement models: the model with anharmonicity of alkaline ion displacements and the split alkaline position model at temperatures higher than 473 K.

It should also be mentioned that the KTP structure type is characterized by a significant amount of weak reflections. Previous studies have been based on X-ray sealed-tube data, which inevitably suffer from low statistical significance of weak reflections. Low resolution of some data also limits the possibility of refining the disordered model unambiguously.

Thus, it was desirable to conduct a supplementary accurate high-flux synchrotron X-ray diffraction study of RTA at room temperature which may assist in understanding the origins of the 'ghosting' phenomenon and the effect of its modelling on the electron density in the KTP type of compounds.

## 2. Experimental

RTA single crystals were grown by spontaneous crystallization from a self-flux, where only constituents of the crystals were present, as described previously by Almgren *et al.* (1999). No impurities in the grown crystals were detected by electron probe microanalysis using a JOEL JXA-8600 Superprobe with

energy- and wavelength-dispersive spectrometers. A small rectangular colourless sample, bounded by the forms {100} and approximately {010} and {001}, was cut from an as-grown plate-like crystal with well developed {100} faces and selected for X-ray diffraction measurements; the dimensions are given in Table 1. Approximation of slightly damaged edges with additional forms did not improve the results. Crystal faces were measured and indexed using both scanning electron and optical microscopy.

Diffraction intensities for $RbTiOAsO_4$ were measured at room temperature with 0.75 Å synchrotron X-radiation using the BL14A four-circle diffractometer (Satow & Iitaka, 1989) at the Photon Factory, Tsukuba, Japan. Although the higher radiation energies would be preferable for studies of the RTA in order to reduce absorption and anomalous scattering, the already fixed energy of 16531 eV was used owing to limited time at the beamline. The energy resolution was estimated to be less than 2 eV and the wavelength was 0.75000 (9) Å. Other reasons for using this wavelength were the greater stability of the experimental equipment at this setting and the higher intensity of radiation to improve measurements of a considerable amount of weak reflections. Vertically polarized X-radiation (polarization ratio $\simeq 0.95$) from a vertical wiggler was monochromated by a double Si(111) perfect crystal monochromator, and focused using a curved fused quartz mirror coated with Pt. The beam optics was automatically adjusted every 20 min to yield maximum flux. A high-speed avalanche photodiode (APD) detector with a counting linearity of up to $10^8$ counts $s^{-1}$ was used (Kishimoto *et al.*, 1998). The experimental set-up was similar to that described by Streltsov *et al.* (1998).

Lattice constants were evaluated from the diffractometer-observed angles for six Friedel pairs [(0 ±12 0), (±24 0 0), (0 0 ±20), (±22 ±6 0), (±24 0 ±8) and (0 ±6 ±20)] at $2\theta$ values in the range given in Table 1. The zero-point correction was determined by centring several reflections at $\pm 2\theta$ values. Reflection intensities were measured systematically using $\omega/2\theta$ continuous time scans with a sampling time of 10 ms per step for a complete sphere of reciprocal space up to $(\sin\theta/\lambda)_{max} = 1.1547$ Å$^{-1}$. The peak scan width, $\omega$, was 0.55°. Intensities for six standard reflections, (±24 0 0), (0 ±12 0) and (0 0 ±20), were remeasured periodically to monitor the incident beam stability. The maximum fluctuation of intensities for the standards was 8.8%. Measured intensities were normalized using the incident beam intensities monitored during each scan. Integrated intensities were further modified and structure-factor variances from counting statistics were adjusted for source instability as indicated by the standards (Rees, 1977). Further experimental details are listed in Table 1.

Lorentz and polarization corrections were applied. Absorption correction factors (Alcock, 1974) were evaluated analytically using linear absorption coefficients at a wavelength of 0.75 Å evaluated from atomic absorption coefficients $\mu/\rho$ (cm$^2$ g$^{-1}$) of 96.9, 26.5, 75.1 and 1.31 for Rb, Ti, As and O, respectively, calculated by Sasaki (1989). The secondary extinction correction for the full data set by techniques based on intensities for symmetry-equivalent reflections with different path lengths (Maslen & Spadaccini, 1993) was attempted. No extinction was detected at this stage. Further attempts to determine the extinction parameter were made during the refinements of structural models. Symmetrically equivalent reflections were averaged keeping Friedel pairs separate. Variances consistent with measurement statistics were retained and those for the other measurements were increased according to the scatter of equivalents following a Fisher test (Hamilton, 1964).

## 3. Least-squares refinements

Details of the different refinement models are given in Table 2.[1] Initially, model I, based on the structural information of RTA at 9 K (Almgren *et al.*, 1999), was optimized. Independent structural parameters, including the scale factor and elements of anisotropic atomic displacement tensors for all atomic sites, were refined by conventional full-matrix least-squares methods including all observed structure factors. The reference state for all structure-factor calculations was the independent atom model (IAM) evaluated using spherical atomic scattering factors with dispersion corrections $\Delta f'$ and $\Delta f''$ of −1.623 and 3.246 for Rb, 0.265 and 0.495 for Ti, −0.147 and 2.204 for As, and 0.0093 and 0.0068 for O at 0.75 Å, calculated by Sasaki (1990). Possible uncertainties in the dispersion corrections should not significantly affect the final results. As shown recently (Streltsov & Ishizawa, 1999) for $HoFe_2$, the scale factor was the only parameter which noticeably changed, while the difference electron density appears to be insensitive to variation of the dispersion corrections. The resulting refinement indexes for model I were $R = 0.026$, $wR = 0.029$ and $S = 2.41$. The residual charge-density maps showed a significant positive density of 4.0 (2) e Å$^{-3}$ near Rb1 and of 1.5 (2) e Å$^{-3}$ near Rb2 at ∼0.5 Å along the $-c$ direction. The positions of these peaks can be related to the main Rb sites by the inversion operation, which were observed previously for other KTP-type materials (Thomas & Womersley, 1998; Belokoneva *et al.*, 1990, 1997; Hansen *et al.*, 1991; Larsen, 1995). This immediately suggests that model I is inadequate for the Rb atoms. Model II, with additional Rb sites, was attempted. The model II refinement converged to $R = 0.023$, $wR = 0.023$ and $S = 1.96$. The occupancies of the Rb split positions are given in Table 3. The total occupancy of the two sets of split positions, respectively, was constrained to be unity during all refinements.

The extinction parameter was also estimated as part of a least-squares optimization of the structural models. The Becker & Coppens (1974) isotropic secondary extinction (type 1) parameter using a Gaussian distribution of the mosaic spread was refined. The minimum extinction correction parameter $y_{min}$ was 0.86 for the 004 reflection (the observed structure factor $F_{obs} = yF_{kin}$, where $F_{kin}$ is the kinematical value of the structure factor). The refined Flack (1983) para-

[1] Supplementary data for this paper are available from the IUCr electronic archives (Reference: OS0048). Services for accessing these data are described at the back of the journal.

**Table 2**
Refinement details.

| | Model I (IAM) | Model II (IAM with split Rb sites) | Model III (IAM with Rb anharmonicity) | Model IV (multipole refinement) | Model V (as IV with split Rb sites) |
|---|---|---|---|---|---|
| Refinement on | *F* | *F* | *F* | *F* | *F* |
| *R* | 0.02647 | 0.02265 | 0.0193 | 0.0211 | 0.0179 |
| *wR* | 0.02840 | 0.02346 | 0.0179 | 0.0213 | 0.0152 |
| *S* | 2.41 | 1.96 | 1.39 | 1.71 | 1.22 |
| No. of reflections used | 5941 | 5941 | 5982 | 5982 | 5982 |
| Variables | 146 | 164 | 195 | 524 | 533 |
| Weighting scheme | $1/\sigma^2(F)$ | $1/\sigma^2(F)$ | $1/\sigma^2(F)$ | $1/\sigma^2(F)$ | $1/\sigma^2(F)$ |
| Extinction method | Becker–Coppens, Type 1, Gaussian | Becker–Coppens, Type 1, Gaussian | Applied from model II | Applied from model II | Applied from model II |
| Extinction coefficient, *r** | 3.0 (1) × $10^5$ | 2.9 (1) × $10^5$ | | | |
| Extintion correction, $y_{min}$ (*hkl*) | 0.85 (004) | 0.86 (004) | | | |
| Flack parameter | 0.424 (3) | 0.424 (3) | Applied from model II | Applied from model II | Applied from model II |
| Source of atomic scattering factors | *International Tables for Crystallography* (1992, Vol. C) | *International Tables for Crystallography* (1992, Vol. C) | Clementi & Roetti (1974) | Clementi & Roetti (1974) | Clementi & Roetti (1974) |

meter of 0.424 (3) suggests that the sample is an almost equal mixture of domains of opposite structural polarity. This is a result of the spontaneous crystal growth at a temperature close to $T_c$ = 1067 K (Marnier *et al.*, 1989). Extinction correction and Flack parameters varied slightly within the s.u. for the model I and model II refinements. It should be noted that the Flack parameter refinement helps to correctly apply the anomalous dispersions, which were then removed from the observed structure factors before further modelling and mapping of the electron density to satisfy the requirement that the electron density is a real quantity. These calculations were based on the *Xtal3.6* system of crystallographic programs (Hall *et al.*, 1999).

The possibility that the strong accumulation of residual density near the Rb atoms is due to anharmonic vibrations of these atoms was then explored. Model I was extended to model III by including a Gram–Charlier expansion (*International Tables for Crystallography*, 1992, Vol. C) to the fourth order of the Rb Debye–Waller factors

$$T(\mathbf{S}) = T_0(\mathbf{S})\left[1 + (i^3/3!)C^{jkl}S_jS_kS_l + (i^4/4!)D^{jklm}S_jS_kS_lS_m\right],$$

where $C^{jkl}$ and $D^{jklm}$ are the third- and the fourth-order coefficients, respectively. The refinement of model III was carried out with the *XD* program system (Koritsanszky *et al.*, 1998) for observed structure factors using absorption, anomalous dispersion and extinction corrections from the model II refinement. The most significant (>20$\sigma$) anharmonic terms were $C^{333}$ = −2.96 (6), $C^{133}$ = 0.61 (3), $C^{233}$ = 0.40 (2) and $D^{3333}$ = 2.1 (3) for Rb1 and $C^{333}$ = −1.28 (4) for Rb2. These terms show that the anharmonicity is more significant in the *c* direction, as expected, and also more pronounced for the Rb1 site. The refinement indexes improved for model III (Table 2); however, significant residual peaks of 2.1 (2) and 1.2 (2) e Å$^{-3}$ near the Rb1 and Rb2 sites, respectively, in the −*c* direction were still observed in the density maps. Moreover, the Rb1 and Rb2 positions were shifted in the −*c* direction resulting in sharp residual features close to the Rb nuclei in the +*c* direction. Therefore, model III was not sufficiently adequate for RTA data at room temperature. This result is similar to that obtained for the anharmonic model refinements for the K atoms in KTP (Delarue *et al.*, 1999) and for the Rb atoms in RTP (Delarue *et al.*, 1998). This suggests that there could be both static (split-position model II) and dynamic (anharmonic model III) disorder of the Rb sites in RTA.

In order to explore whether the accumulation of residual density near the Rb atoms is entirely due to asphericity of the electron distribution, the refinement of model IV was attempted. Model IV was an extension of model I so as to include multipole parameters up to *l* = 4 (hexadecapoles) along with the scale factor and conventional atomic parameters for all atoms. The aspherical atomic electron density is divided into three components according to the formalism of

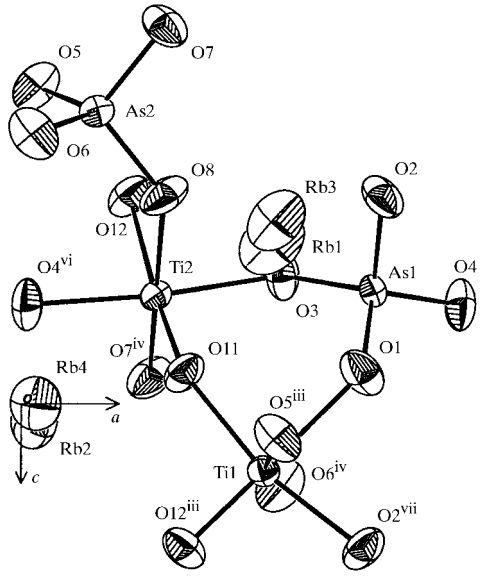


**Figure 1**
*ORTEP* view of the structure. Displacement ellipsoids are shown at the 99% probability level. Symmetry codes are given in Table 4.

**Table 3**
Fractional atomic coordinates and equivalent ($U_{eq}$, Å$^2$) and anisotropic ($U^{ij}$, Å$^2$) displacement parameters, $U_{eq} = (1/3)\Sigma_i\Sigma_j U^{ij} a^i a^j \mathbf{a}_i.\mathbf{a}_j$.

| | $x$ | $y$ | $z$ | $U_{eq}$ | Occupancy |
|---|---|---|---|---|---|
| Rb1 | 0.38246 (4) | 0.78159 (6) | 0.70236 (3) | 0.017 | 0.885 (5) |
| Rb2 | 0.10885 (6) | 0.69335 (10) | 0.95521 (4) | 0.014 | 0.872 (9) |
| Rb3 | 0.3871 (2) | 0.7878 (4) | 0.6741 (2) | 0.014 | 0.115 (5) |
| Rb4 | 0.1110 (4) | 0.6983 (5) | 0.9340 (3) | 0.011 | 0.128 (9) |
| Ti1 | 0.373747 (13) | 0.505054 (29) | 1.027988 (17) | 0.005 | |
| Ti2 | 0.248776 (15) | 0.269988 (26) | 0.777903 (18) | 0.005 | |
| As1 | 0.499652 (9) | 0.328210 (14) | 0.770681 (13) | 0.004 | |
| As2 | 0.179890 (7) | 0.505071 (17) | 0.516443 (11) | 0.005 | |
| O1 | 0.48731 (8) | 0.48947 (16) | 0.88714 (9) | 0.011 | |
| O2 | 0.51039 (7) | 0.46126 (15) | 0.63784 (8) | 0.010 | |
| O3 | 0.39509 (6) | 0.18744 (14) | 0.74880 (9) | 0.009 | |
| O4 | 0.60025 (6) | 0.17655 (14) | 0.79062 (9) | 0.009 | |
| O11 | 0.28160 (7) | 0.45211 (14) | 0.88764 (8) | 0.008 | |
| O12 | 0.21791 (7) | 0.05542 (14) | 0.63748 (8) | 0.009 | |
| O5 | 0.10983 (8) | 0.30341 (13) | 0.48072 (9) | 0.009 | |
| O6 | 0.10713 (8) | 0.70414 (13) | 0.54832 (10) | 0.010 | |
| O7 | 0.25824 (8) | 0.54470 (15) | 0.39454 (9) | 0.010 | |
| O8 | 0.25779 (8) | 0.45857 (15) | 0.63651 (8) | 0.010 | |

| | $U^{11}$ | $U^{22}$ | $U^{33}$ | $U^{12}$ | $U^{13}$ | $U^{23}$ |
|---|---|---|---|---|---|---|
| Rb1 | 0.02131 (9) | 0.00722 (6) | 0.02104 (12) | 0.00289 (5) | −0.00609 (11) | −0.00211 (9) |
| Rb2 | 0.01048 (8) | 0.01382 (10) | 0.01740 (17) | 0.00368 (6) | −0.00058 (12) | −0.00088 (10) |
| Rb3 | 0.0159 (5) | 0.0073 (5) | 0.0181 (8) | 0.0028 (3) | −0.0055 (7) | −0.0020 (6) |
| Rb4 | 0.0107 (5) | 0.0065 (4) | 0.0147 (9) | 0.0019 (3) | 0.0010 (7) | −0.0006 (6) |
| Ti1 | 0.00519 (5) | 0.00489 (5) | 0.00490 (5) | −0.00005 (5) | 0.00018 (4) | −0.00091 (5) |
| Ti2 | 0.00502 (4) | 0.00500 (5) | 0.00473 (5) | −0.00028 (5) | −0.00064 (5) | 0.00014 (5) |
| As1 | 0.00378 (3) | 0.00446 (3) | 0.00510 (3) | −0.00004 (3) | 0.00065 (2) | −0.00029 (3) |
| As2 | 0.00624 (3) | 0.00344 (3) | 0.00513 (3) | −0.00027 (3) | −0.00029 (3) | 0.00061 (2) |
| O1 | 0.0100 (3) | 0.0117 (3) | 0.0105 (3) | −0.0033 (2) | 0.0038 (2) | −0.0062 (2) |
| O2 | 0.0087 (3) | 0.0117 (3) | 0.0091 (2) | 0.0020 (2) | 0.0031 (2) | 0.0047 (2) |
| O3 | 0.0058 (2) | 0.0073 (2) | 0.0127 (3) | −0.0015 (2) | 0.0005 (2) | −0.0019 (2) |
| O4 | 0.0048 (2) | 0.0088 (2) | 0.0138 (3) | 0.0011 (2) | −0.0005 (2) | 0.0024 (2) |
| O11 | 0.0082 (2) | 0.0090 (2) | 0.0078 (2) | 0.0005 (2) | −0.0027 (2) | −0.0031 (2) |
| O12 | 0.0092 (3) | 0.0092 (3) | 0.0085 (2) | 0.0005 (2) | −0.0031 (2) | −0.0022 (2) |
| O5 | 0.0116 (3) | 0.0048 (2) | 0.0119 (3) | −0.0018 (2) | −0.0039 (2) | 0.0007 (2) |
| O6 | 0.0123 (3) | 0.0053 (2) | 0.0139 (3) | 0.0009 (2) | 0.0038 (2) | −0.0003 (2) |
| O7 | 0.0106 (3) | 0.0103 (3) | 0.0090 (2) | 0.0032 (2) | 0.0031 (2) | 0.0045 (2) |
| O8 | 0.0117 (3) | 0.0110 (3) | 0.0081 (2) | −0.0039 (2) | −0.0043 (2) | 0.0044 (2) |

Hansen & Coppens (1978) implemented in the *XD* program system

$$\rho(\mathbf{r}) = \rho_{core}(r) + P_{val}\, k^3 \rho_{val}(kr) + \sum_{l=0}^{4} k'^3 R_{n_l}(k'r) \sum_{m=0}^{l} P_{pm\pm}\, y_{lm\pm}(\theta, \varphi),$$

where $\rho_{core}$ and $\rho_{val}$ are spherically averaged core and valence densities, respectively, $y_{lm\pm}$ are the multipolar spherical harmonic angular functions in real form and $R_{nl}(k'r)$ are exponential-type radial functions. The expansion–contraction parameters $k$ and $k'$ of the pseudo-atomic charge density were also included in refinement. The two independent Rb atoms were refined as $Rb^+$ ions (Kr core scattering factors), and the residual two electrons were distributed (equally at the beginning of refinement) over the O atoms to satisfy the unit-cell electroneutrality. No other constraints were applied. The fit indexes were worse than those for model III but slightly better than those for model II. However, the peaks of 2.9 (2) and 0.4 (2) e Å$^{-3}$ at the 'ghost' Rb sites were still observed in the residual charge-density maps after the refinement of model IV. The lowest residual density for those peaks was obtained with model II. Therefore, in order to obtain better representation of the charge density for the non-centrosymmetric RTA structure, the Rb split positions as in model II and the multipole functions for the other atoms as in model IV were employed in further refinements. The occupancies of the extra two positions of Rb were fixed according to the model II refinement. The final model V refinement converged to the lowest values of $R$ = 0.0179, $wR$ = 0.0152 and $S$ = 1.22. The fractional coordinates and atomic displacement parameters from the model V refinement are given in Table 3 and selected bond distances are given in Table 4.

## 4. Structural parameters

The crystal structure of RTA at room temperature and at 9 K was described by Almgren *et al.* (1999). All atoms are on general positions in the unit cell, which contains eight formula units. An *ORTEP* (Johnson *et al.*, 1972) plot of the studied RTA structure is given in Fig. 1. It can be described as a three-dimensional network of $AsO_4$ tetrahedra and distorted $TiO_6$ octahedra with shared corners and with $AsO_4$—$TiO_6$—$AsO_4$—$TiO_6$ chains along the [100], [010] and [101] directions. These chains form helical channels along the $c$ axis in which the Rb cations are located. The O11 and O12 atoms connect the octahedra forming zigzag $TiO_6$ chains along the [011] and [0$\bar{1}$1] directions. The Ti atoms are displaced from their ideal positions in the $TiO_6$ octahedra forming short Ti1—O12 and Ti2—O11 bonds, opposing long bonds and intermediate bonds.

The average fractional $z$-coordinates of 0.6882 (2) for Rb1 and Rb3 and of 0.9446 (3) for Rb2 and Rb4 from Table 3 are very close to those of 0.68708 (6) and 0.93924 (6) observed in RTA at 9 K (Almgren *et al.*, 1999). This suggests that when the temperature decreases the split Rb positions converge to that observed at 9 K, which is close to the centre of mass of two extra sites. An attempt to refine the split Rb sites at 9 K was unsuccessful, owing to strong correlation between structural and occupancy parameters (Almgren *et al.*, 1999). The Rb1—

Rb3 and Rb2—Rb4 distances are 0.312 (3) and 0.233 (4) Å, respectively, approximately along the *c* axis. These distances are longer than those of 0.27 (1) and 0.19 (1) Å reported by Delarue *et al.* (1998) for $RbTiPO_4$ at 473 K. The average shift of the additional positions from the main Rb sites in RTA is approximately 0.27 Å in the $-c$ direction. The optical criterion for the resolution of the electron-density Fourier series (*e.g.* James, 1982) suggests that details of the electron density on a larger scale than $r = 0.61/(2\sin\theta/\lambda)_{max} = 0.26$ Å can be resolved.

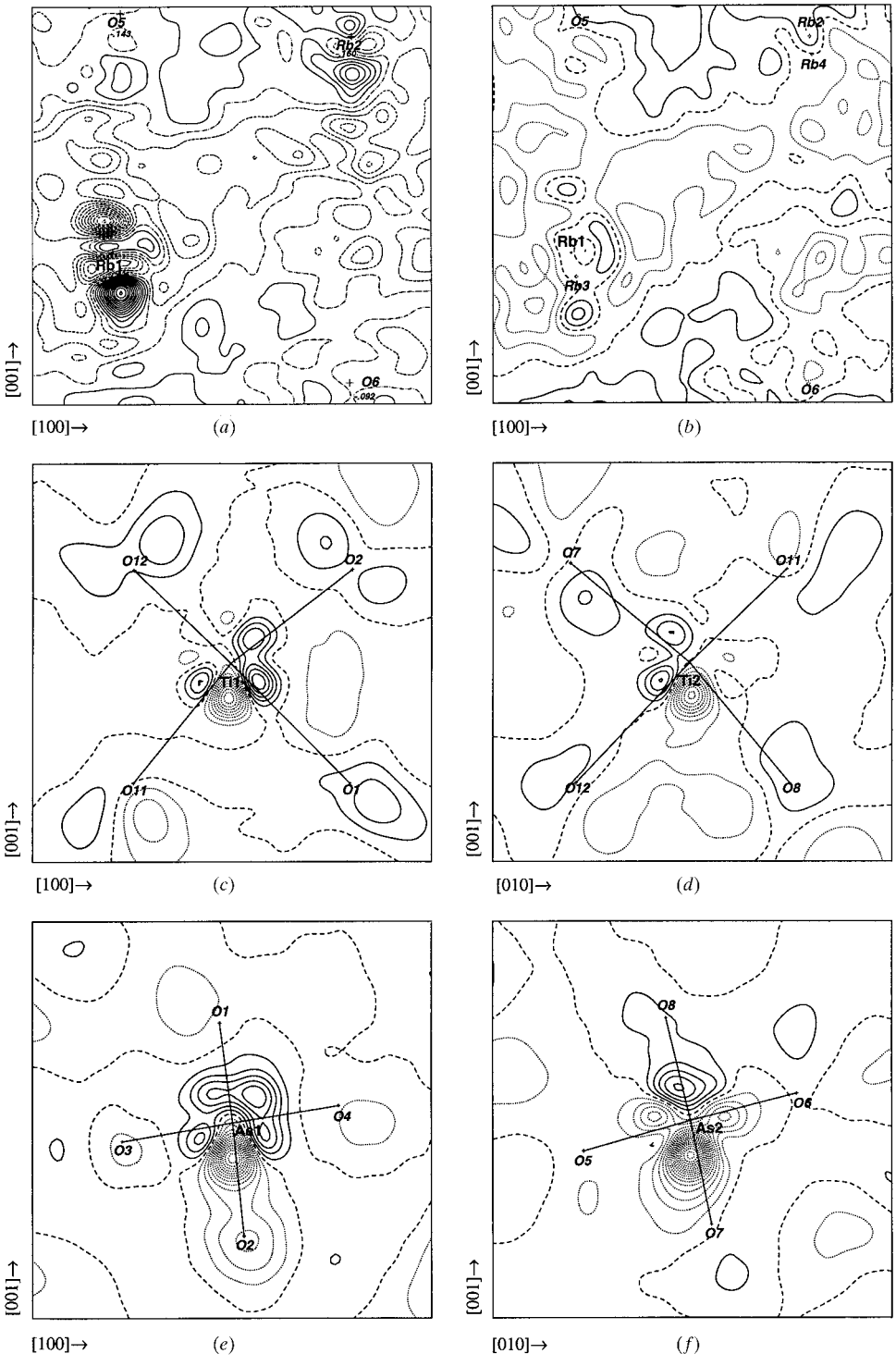


**Figure 2**
Difference density maps: $\Delta\rho$ in the (010) plane through Rb1 for (*a*) model I and (*b*) model V refinements and $\Delta\rho_M$ in (*c*) the (010) plane through Ti1, (*d*) the (100) plane through Ti2, (*e*) the (010) plane through As1, and (*f*) the (100) plane through As2. Contour intervals are 0.3 e Å$^{-3}$ [$\sigma(\Delta\rho) = 0.2$ e Å$^{-3}$]; positive contours are solid and negative contours are shown as short dashed lines. Atoms deviating from the planes are shown in italics. Map borders are 5 × 5 Å.

## 5. Charge density

Atomic charges of +0.18 (6), +0.21 (7), +2.59 (3), +1.81 (2) and −0.68 (9) e for Ti1, Ti2, As1, As2 and average O, respectively, have been calculated from the monopole populations of the model V refinement. It should be mentioned that during the model V refinement the unit cell was constrained to be neutral, and the charges of Rb atoms were fixed to +1. The signs of charges are in accordance with the atomic electronegativities; however, the values are quite far from formal ionic charges reflecting the covalency of the chemical bonds. It should be noted that the crystallographically independent Ti1 and Ti2 cations have similar charges which are also close to those of +0.5 (5) e previously reported in RTA at 9 K using Hirshfeld partitioning.

Although realizing that the sample studied appears to be a polar twin according to the Flack parameter value, the difference density analysis was nevertheless attempted. The Flack parameter refinement should essentially reduce the effect of domains of opposite structural polarity on the density maps. It should also be noted that the KTP sample in which the charge density was studied by Hansen *et al.* (1991) behaved as a polar twin according to the reported refinement of the Rogers parameter (Rogers, 1981).

Figs. 2(*a*) and (*b*) show the difference charge density ($\Delta\rho = \rho_{exp} - \rho_{IAM}$) sections in

**Table 4**
Bond distances (Å).

| | | | |
|---|---|---|---|
| Rb1—Rb3 | 0.312 (3) | Ti2—O11 | 1.7476 (8) |
| Rb2—Rb3$^{i}$ | 3.585 (3) | Ti2—O12 | 2.1192 (9) |
| Rb2—Rb4 | 0.233 (4) | Ti2—O7$^{i}$ | 1.9586 (9) |
| Rb3—Rb4$^{ii}$ | 3.762 (4) | Ti2—O8 | 1.9760 (9) |
| Ti1—O1 | 2.1358 (9) | As1—O1 | 1.6581 (8) |
| Ti1—O2$^{iii}$ | 1.9484 (9) | As1—O2 | 1.6869 (8) |
| Ti1—O11 | 1.9716 (8) | As1—O3 | 1.6885 (9) |
| Ti1—O12$^{iv}$ | 1.7232 (8) | As1—O4 | 1.6855 (8) |
| Ti1—O5$^{iv}$ | 2.0644 (9) | As2—O5 | 1.6777 (9) |
| Ti1—O6$^{i}$ | 2.0337 (8) | As2—O6 | 1.6751 (9) |
| Ti2—O3 | 2.0374 (9) | As2—O7 | 1.6917 (9) |
| Ti2—O4$^{v}$ | 2.0025 (8) | As2—O8 | 1.6806 (9) |

Symmetry codes: (i) $\frac{1}{2}-x, y-\frac{1}{2}, \frac{1}{2}+z$; (ii) $\frac{1}{2}-x, \frac{1}{2}+y, z-\frac{1}{2}$; (iii) $1-x, 1-y, \frac{1}{2}+z$; (iv) $\frac{1}{2}-x, \frac{1}{2}+y, \frac{1}{2}+z$; (v) $x-\frac{1}{2}, \frac{1}{2}-y, z$.

the (010) plane through the Rb1 atom calculated for models I and V, respectively. The 0.3 e Å$^{-3}$ contour intervals are greater than the mean of $\sigma(\Delta\rho)$ = 0.2 e Å$^{-3}$ (Maslen, 1988). The significant accumulation of electron density near Rb1 and Rb2 at a distance of ~0.5 Å along –**c** in Fig. 2(*a*) was almost completely accounted for by the two additional independent Rb sites (Rb3 and Rb4), as shown in Fig. 2(*b*).

Figs. 2(*c*)–(*f*) depict the model difference charge density ($\Delta\rho_M = \rho_{\text{model V}} - \rho_{\text{IAM}}$) maps calculated using the model V parameters. The difference density features near the Ti atoms in Figs. 2(*c*) and (*d*) are dissimilar to those obtained in RTA at 9 K using the conventional IAM refinement. The previously observed features did not correspond to the Ti—O geometry but showed dipole-like density oriented parallel to the *c* axis. Those features changed when the difference density maps (Figs. 2*c* and *d*) were calculated using the phases from the model V multipole refinement. A similar effect was observed by Hansen *et al.* (1991) for $KTiPO_4$. This emphasizes the importance of thorough non-spherical density models for non-centrosymmetric structures.

Furthermore, the excess charge density near Ti1 in Fig. 2(*c*) tends to be along the longer Ti1—O1 [2.1358 (9) Å] and intermediate Ti1—O2 [1.9484 (9) Å] and Ti1—O11 [1.9716 (8) Å] bonds, avoiding the shortest Ti1—O12 [1.7232 (8) Å] bond. Similarly, in the Ti2—O octahedron in Fig. 2(*d*) the density is concentrated along the longest Ti2—O12 [2.1192 (9) Å] and the intermediate Ti2—O7 [1.9586 (9) Å] bonds, and is within one contour interval along the shorter Ti2—O11 [1.7476 (8) Å] bond. It should be noted that the O12 and O11 atoms connect two Ti octahedra and form alternating shorter (Ti1—O12 and Ti2—O11) and longer (Ti2—O12 and Ti1—O11) bond chains along the polar *c* axis. The excess charge density is observed in the longer bonds in these chains.

Figs. 2(*e*) and (*f*) present the $\Delta\rho_M$ density in the (010) and (100) planes through the As1 and As2 atoms, respectively. In general, the maps in the As1 and As2 tetrahedra show similar features. The charge densities near the As atoms show strong dipole and octupole terms along the +*c* axis. The excess densities are also slightly shifted along the As1—O1 and As2—O8 bonds, while the As1—O2 and As2—O7 directions are depleted. It is interesting to note that these bonds alternate the long Ti1—O1 and the intermediate Ti1—O2, Ti2—O7 and Ti2—O8 bonds forming the short/long bond chains in the *c* direction. Similar to the Ti—O—Ti—O chains discussed above, the excess density in the longer Ti1—O2 bond alternates the depleted density in the shorter As1—O2 bond. This is less obvious for the Ti1—O1—As1 part of the chain, where Ti1—O1 is the longest bond. However, the Ti—O7—As2—O8—Ti2 chain has a well pronounced excess/depletion 'density wave'.

It is interesting to note that the observed charge-density features of the Ti—O—Ti—O and Ti—O—As—O chains can be related to the bond-polarization theory predictions (Levine, 1974). Theory predicts that, for covalent bonds, as length increases and the atom cores are separated further apart the effective potential acting on the mobile bonding electrons decreases, thereby increasing both linear and non-linear polarizibilites. The accumulated electrons in the areas of longer covalent bonds with lower potentials in the bonding areas are loosely bound and should increase the optic response. Strong polarization of $\Delta\rho$ along short and long periodic bonding chains in the polar *c* direction suggests that there is charge transfer along these chains, which is favourable for the non-linear optical properties which are more pronounced in the *c* direction. Thus, it can be speculated that the observed charge density reflects the anisotropy of non-linear susceptibility in this type of structure. The non-linear susceptibility is larger for directions where locally antisymmetric components of $\Delta\rho$ are strong.

The authors are grateful to Dr N. Ishizawa for assistance during data collection and Professor B. N. Figgis for permission to use the *XD* program implemented on the UWA Chemistry Department computers. This work was supported by the Australian Research Council. Financial support from the Australian Synchrotron Research Program funded by the Commonwealth of Australia *via* the Major National Research Facilities Program is also acknowledged.

## References

Alcock, N. W. (1974). *Acta Cryst.* A**30**, 332–335.
Almgren, J., Streltsov, V. A., Sobolev, A. N., Figgis, B. N. & Albertsson, J. (1999). *Acta Cryst.* B**55**, 712–720.
Becker, P. J. & Coppens, P. (1974). *Acta Cryst.* A**30**, 148–153.
Belokoneva, E. L., Knight, K. S., David, W. I. F. & Mill, B. V. (1997). *J. Phys. Condens. Matter*, **9**, 3833–3851.
Belokoneva, E. L., Yakubovich, O. V., Tsirelson, V. G. & Urusov, V. S. (1990). *Izv. Akad. Nauk SSSR Neorg. Mater.* **26**, 595–601.
Clementi, E. & Roetti, C. (1974). *At. Data Nucl. Data Tables*, **14**, 177–478.
Dahaoui, S., Hansen, N. K., Protas, J., Krane, H.-G., Fischer, K. & Marnier, G. (1999). *J. Appl. Cryst.* **32**, 1–10.
Delarue, P., Lecomte, C., Jannin, M., Marnier, G. & Menaert, B. (1998). *Phys. Rev. B*, **58**, 5287–5295.
Delarue, P., Lecomte, C., Jannin, M., Marnier, G. & Menaert, B. (1999). *J. Phys. Condens. Matter*, **11**, 4123–4134.
Flack, H. D. (1983). *Acta Cryst.* A**39**, 876–881.

Hall, S. R., du Boulay, D. J. & Olthof-Hazekamp, R. (1999) Editors. *Xtal3.6 Reference Manual.* University of Western Australia, Australia.
Hamilton, W. C. (1964). *Statistics in Physical Science.* New York: Ronald Press.
Hansen, N. K. & Coppens, P. (1978). *Acta Cryst.* A**34**, 909–921.
Hansen, N. K., Protas, J. & Marnier, G. (1991). *Acta Cryst.* B**47**, 660–672.
Hu, Z. W., Thomas, P. A., Webjörn, J. & Loiacono, G. M. (1996). *J. Phys. D*, **29**, 1681–1684.
James, R. W. (1982). *The Optical Principles of the Diffraction of X-rays*, p. 400. Woodbridge, Connecticut: Ox Bow Press.
Johnson, C. K., Guerdon, J. F., Richard, P., Whitlow, S. & Hall, S. R. (1972). *ORTEP. The X-ray System of Crystallographic Programs.* Technical Report TR-192. Computer Science Centre, University of Maryland, College Park, Maryland, USA.
Karlsson, H., Laurell, F., Henriksson, P. & Arvidsson, G. (1996). *Electron. Lett.* **32**, 556–557.
Kishimoto, S., Ishizawa, N. & Vaalsta, T. P. (1998). *Rev. Sci. Instrum.* **69**, 384–391.
Koritsanszky, T., Howard, S., Mallison, P. R., Su, Z., Richter, T. & Hansen, N. (1998). *XD. A Computer Program Package for Multipole Refinement and Analysis of Charge Densities from Diffraction Data.* Institute of Crystallography, Berlin, Germany.
Larsen, F. K. (1995). *Acta Cryst.* B**51**, 468–482.
Levine, B. F. (1974). *Phys. Rev. B*, **10**, 1655–1664.
Mangin, J., Marnier, G., Boulanger, B. & Menaert, B. (1989). *Inst. Phys. Conf. Ser.* **103**, 65–68.
Marnier, G., Boulanger, B. & Menaert, B. (1989). *J. Phys. Condens. Matter*, **1**, 5509–5513.
Maslen, E. N. (1988). *Acta Cryst.* A**44**, 33–37.
Maslen, E. N. & Spadaccini, N. (1993). *Acta Cryst.* A**49**, 661–667.
Rees, B. (1977). *Isr. J. Chem.* **16**, 180–186.
Risk, W. P. & Loiacono, G. M. (1996). *Appl. Phys. Lett.* **69**, 311–313.
Rogers, D. (1981). *Acta Cryst.* A**37**, 734–741.
Sasaki, S. (1989). *Numerical Tables of Anomalous Scattering Factors, Calculated by the Cromer and Mann's Method.* KEK Report 88–14, 1–136. KEK, Tsukuba, Japan.
Sasaki, S. (1990). *X-ray Absorption Coefficients for the Elements (Li to Bi, U).* KEK Report 90–16, 1–143. KEK, Tsukuba, Japan.
Satow, Y. & Iitaka, Y. (1989). *Rev. Sci. Instrum.* **60**, 2390–2393.
Stefanovich, S., Mosunov, A., Mill, B. & Belokoneva, E. (1996). *Ferroelectrics*, **185**, 63–66.
Streltsov, V. A. & Ishizawa, N. (1999). *Acta Cryst.* B**55**, 321–326.
Streltsov, V. A., Ishizawa, N. & Kishimoto, S. (1998). *J. Synchrotron Rad.* **5**, 1309–1316.
Thomas, P. A., Glazer, A. M. & Watts, B. E. (1990). *Acta Cryst.* B**46**, 333–343.
Thomas, P. A. & Womersley, M. N. (1998). *Acta Cryst.* B**54**, 645–651.
Womersley, M. N., Thomas, P. A. & Corker, D. L. (1998). *Acta Cryst.* B**54**, 635–644.